Available online at www.sciencedirect.com
SCIENCE DIRECT®
Journal of Molecular Catalysis A: Chemical 238 (2005) 1–12
JOURNAL OF MOLECULAR CATALYSIS A: CHEMICAL
www.elsevier.com/locate/molcata

A dimeric molecular precursor $[(^tBuO)_2Ti\{\mu\text{-}O_2Si[OSi(O^tBu)_3]_2\}]_2$ to $Ti(IV)/SiO_2$ catalysts for selective cyclohexene epoxidation

Richard L. Brutchey [a,b], Benjamin V. Mork [a,b], Donald J. Sirbuly [a,b], Peidong Yang [a,b], T. Don Tilley [a,b,*]

[a] *Department of Chemistry, University of California at Berkeley, Berkeley, CA 94720-1460, USA*
[b] *Chemical Sciences Division, Lawrence Berkeley National Laboratory, 1 Cyclotron Road, Berkeley, CA 94720, USA*

Received 5 February 2005; received in revised form 2 April 2005; accepted 20 April 2005
Available online 14 June 2005

Abstract

The new dimeric complex $[(^tBuO)_2Ti\{\mu\text{-}O_2Si[OSi(O^tBu)_3]_2\}]_2$ (**1**), prepared via silanolysis of $Ti(O^tBu)_4$ with $(HO)_2Si[OSi(O^tBu)_3]_2$, is a structural and spectroscopic (NMR, FT-IR, UV–vis, XPS) model for $Ti(IV)/SiO_2$. The molecular complex was used to prepare titanium-containing silica materials through both the thermolytic molecular precursor method (yielding $TiO_2{\cdot}3SiO_2$) or by grafting **1** onto mesoporous SBA-15 silica. Grafting **1** onto SBA-15 yields mostly isolated Ti(IV) sites, as evidenced by DRUV–vis and photoluminescence spectroscopies. The resulting materials were found to be active and highly selective in the epoxidation of cyclohexene, yielding up to 71% of cyclohexene oxide based on oxidant (cumene hydroperoxide) after 2 h at 65 °C in toluene.

Keywords: Titanium; Molecular precursor route; Supported catalysts; Epoxidation; Peroxides

1. Introduction

Since the development of a heterogeneous silica-supported titanium epoxidation catalyst by Shell in the 1970s [1], there has been considerable attention given to $Ti(IV)/SiO_2$ catalytic materials. A multitude of $Ti(IV)/SiO_2$ materials have been studied for the catalytic oxidation of hydrocarbons—including, but not limited to, TS1 and TS2 (titanium-substituted molecular sieves) [2–4], Ti-β (titanium-substituted zeolite) [5,6], and Ti-SBA15 and Ti-MCM41 (titanium substituted into or grafted onto mesoporous silica) [7–10]. It is established that the most active and selective oxidation catalysts contain isolated, four-coordinate Ti(IV) centers accessible on the surface of the silica to the hydrocarbon substrate [11–13]. Consequently, a substantial amount of work has focused on the conversion of discrete molecular precursors to yield homogeneous $Ti(IV)/SiO_2$ materials with a high abundance of isolated, four-coordinate Ti(IV) [14–20].

Our previous research on titania–silica focused on the oxygen-rich molecular precursor $Ti[OSi(O^tBu)_3]_4$ and its thermolytic conversion to a $TiO_2{\cdot}4SiO_2$ material by the

$$Ti[OSi(O^tBu)_3]_4 \xrightarrow[200\,^\circ C]{\text{toluene}} TiO_2 \cdot 4SiO_2 + 12H_2C{=}CMe_2 + 6H_2O \quad (1)$$

facile elimination of isobutylene and water (Eq. (1)) [21]. The resulting $TiO_2{\cdot}4SiO_2$ materials have a homogeneous distribution of titanium in the silica matrix that appears to result from the preformed Ti–O–Si linkages in the molecular precursor. Also, since the thermolytic conversion of $Ti[OSi(O^tBu)_3]_4$ can be carried out in non-polar media, high surface area $TiO_2{\cdot}4SiO_2$ xerogels (ca. 500 $m^2\,g^{-1}$) are produced upon processing. These xerogels demonstrated moderate to excellent catalytic activities for the epoxidation of cyclohexene to cyclohexene oxide using *tert*-butyl hydroperoxide (TBHP) or cumene hydroperoxide (CHP) as oxidants. In addition to amorphous $TiO_2{\cdot}4SiO_2$ xerogels, low weight loadings of $Ti[OSi(O^tBu)_3]_4$ can be grafted onto a silica surface to give

* Corresponding author. Tel.: +1 5106437970; fax: +1 5106428940.
E-mail address: tdtilley@berkeley.edu (T.D. Tilley).

1381-1169/$ – see front matter © 2005 Elsevier B.V. All rights reserved.
doi:10.1016/j.molcata.2005.04.032

single-site titanium that is catalytically active and selective in the epoxidation of cyclohexene using TBHP or CHP as oxidants (Eq. (2)) [22,23].

It is of interest to study how the molecular structure of the precursor complexes affects the catalytic properties of the resultant materials. One such structural change of interest is use of a dimeric Ti(IV) source instead of a monomeric source. This report describes the synthesis of a series of Ti(IV)/SiO_2 materials using the new dititanium

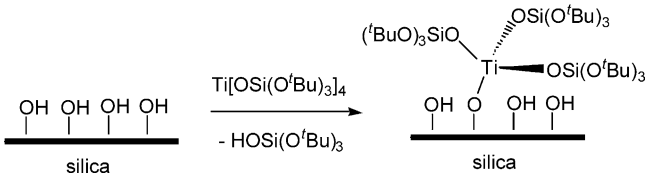

(2)

molecular precursor $[(^tBuO)_2Ti\{\mu\text{-}O_2Si[OSi(O^tBu)_3]_2\}]_2$ (**1**), and the behavior of these materials as cyclohexene epoxidation catalysts. The molecular precursor **1** was also grafted onto the surface of mesoporous silica (SBA-15) to give isolated Ti(IV) catalytic centers, and the effect of grafting a dimeric Ti(IV) source was probed.

2. Experimental procedures

2.1. General procedures

All manipulations were conducted under a nitrogen atmosphere using standard Schlenk techniques or in a vacuum atmospheres drybox, unless otherwise noted. Dry, oxygen-free solvents were used throughout. Benzene-d_6 was purified and dried by vacuum distillation from sodium/potassium alloy.

$Ti(O^tBu)_4$ was purchased from Strem Chemicals, Inc. and distilled prior to use. $[(^tBuO)_3SiO]_2Si(OH)_2$ was prepared as described in the literature [24]. Cyclohexene was purchased from Aldrich and distilled prior to use. CHP (80%) and TBHP (5.5 M in decane) were purchased from Aldrich and used as received. SBA-15 was prepared as described in the literature [25].

2.2. Synthesis of $[(^tBuO)_2Ti\{\mu\text{-}O_2Si[OSi(O^tBu)_3]_2\}]_2$ (1)

A pentane (20 mL) solution of $[(^tBuO)_3SiO]_2Si(OH)_2$ (0.973 mmol) was added to a pentane (10 mL) solution of $Ti(O^tBu)_4$ (0.924 mmol) in a Schlenk tube under flowing nitrogen at 0 °C. The tube was warmed to room temperature and the reaction mixture was stirred for 15 h. Subsequent removal volatile material under vacuum (25 °C) yielded a white solid. The white solid was dissolved in a pentane/toluene (ca. 1:1, v/v) solvent mixture (10 mL) and kept at −78 °C for 72 h. Analytically pure colorless crystals were isolated at −78 °C (73%). Anal. Calcd for $C_{64}H_{144}O_{24}Si_6Ti_2$ (%): C, 49.2; H, 9.23. Found: C, 49.0; H, 9.49. FT-IR (KBr, cm^{-1}): 2975 vs, 2931 m, 2874 w, 1473 vw, 1389 m, 1345 s, 1241 s, 1193 s, 1068 vs, 1026 s, 974 vs, 832 w, 797 w, 760 vw, 702 w, 648 vw, 616 vw, 558 vw, 506 vw, 481 w, 431 vw. ^{1}H NMR (benzene-d_6, 25 °C, 400 MHz): δ 1.59 (s, $Si(O^tBu)_3$), 1.55 (s, $Ti(O^tBu)_3$). $^{13}C\{^1H\}$ NMR (benzene-d_6, 25 °C, 100 MHz): δ 84.3 ($TiOCMe_3$), 73.3 ($SiOCMe_3$), 32.9 ($TiOCMe_3$), 32.7 ($SiOCMe_3$). ^{29}Si MAS NMR (25 °C, 99 MHz): δ −100 ($Si(O^tBu)_3$), −116 ($Si(OTi)_2$).

2.3. Gelation of 1 in toluene [TiO_2·3SiO_2]

A 6.0 mL toluene solution of **1** (0.564 g, 0.060 M) was sealed in a 20 mL Parr reactor in a drybox under a nitrogen atmosphere. The reactor was placed in a preheated oven (180 °C) for 24 h. The wet gel was removed and air-dried for 1 week to form a xerogel. The xerogel was rinsed with pentane (2 × 5 mL) and toluene (2 × 5 mL) and was allowed to air dry for 1 day. The off-white xerogel was ground into a fine powder and dried in vacuo for 12 h at 120 °C to yield 0.174 g of material. Repeated syntheses of TiO_2·3SiO_2 provided materials with similar carbon and hydrogen contents, and the same surface areas (within experimental error).

2.4. Ti_2SBA15(x) preparation

The SBA-15 was dried at 130 °C in vacuo for 15 h and thereafter handled under a nitrogen atmosphere. A 0.5 g sample of SBA-15 was suspended in pentane (25 mL). A pentane solution (30 mL) of **1** was prepared, the concentration of which depended on the desired Ti loading (1.32 wt% loading to yield 0.17 wt% and 2.64 wt% loading to yield 1.58 wt%). The pentane solution of **1** was then added to the stirred suspension of SBA-15 (25 °C). The resulting mixture was stirred for 15 h and then filtered and washed with pentane (3 × 20 mL). The grafted material was dried for 2–3 h in vacuo to yield the as prepared catalyst.

2.5. Catalysis procedure

A sample of catalyst (0.035 g) was added to a 50 mL round-bottom flask that was fitted with a reflux condenser and a septum. Toluene (5.0 mL) and cyclohexene (2.5 mL) were added by syringe through the septum under a flow of nitrogen. Dodecane (50.0 μL) was added as an internal standard. The mixture was allowed to equilibrate at the reaction temperature of 65 °C for 10 min. CHP (1.0 mL) or TBHP (1.0 mL) was added by syringe to the rapidly stirring solution. Aliquots (ca. 0.08 mL) were removed from the reaction mixture by syringe after 5, 30, 60, 90, and 120 min and then filtered and cooled. The filtrate was analyzed by GC, and assignments were made by comparison with authentic samples analyzed under the same conditions.

2.6. Characterization

Solution ^{1}H NMR spectra were recorded at 400 MHz using a Bruker AM-400 spectrometer and were referenced internally to the residual solvent proton signal relative to tetramethylsilane. ^{29}Si CP MAS NMR data were collected on a CMX400 Infinity spectrometer based on a 9.4 T magnet, with a frequency of 79.4867 MHz, spectrum width of 50 kHz, 90° pulse length of 8 μs, contact time of 2–3 ms, and pulse delay of 5 s. Tetramethylsilane was used as an external chemical shift reference and samples were spun at 3.2–3.5 kHz. Infrared spectra were recorded as KBr disks using a Mattson FT-IR spectrometer. Elemental analyses were performed by the College of Chemistry microanalytical laboratory at the University of California, Berkeley or by Galbraith Laboratories. PXRD experiments were performed on a Siemens D5000 X-ray diffractometer using Cu Kα radiation. Transmission electron microscopy was carried out on a Topcon EM-002B transmission electron microscope operating at 200 kV. Samples for energy-dispersive spectroscopy (EDS) were studied on a Phillips CM-200 transmission electron microscope operating at 200 kV. EDS spectra were taken on a Gatan detector connected to the electron microscope. Samples for TEM studies were prepared by depositing a pentane suspension of the finely ground xerogels onto carbon-coated copper grids obtained from Ted Pella, Inc. DRUV–vis spectra were acquired using a Perkin-Elmer Lambda-9 spectrophotometer equipped with a 60 mm integrating sphere (ratio of apertures to sphere surface ca. 8%), a slit width of 4 nm, and collection speed of 120 nm min^{-1}. Samples were run using $BaSO_4$ as the reference material. XPS was performed on a Physical Electronics PHI 5400 ESCA using a Mg anode X-ray source. Photoluminescence measurements were performed using a CW laser source (HeCd, 325 nm). The excitation source was focused on the samples at an incidence angle of 35° to the substrate plane for the HeCd. Light emitted from the sample was collected using a 50× microscope objective (Nikon, 0.7NA) positioned above the sample, and redirected to a fiber optic coupled to a liquid nitrogen cooled CCD/spectrometer (Roper Scientific). The spectral resolution for the PL data shown here is about 0.4 nm. Samples were placed in a microscope cryostat (Janis, ST-500H) equipped with a fused-silica excitation port for both room and low temperature PL measurements. A thin film of Crycon thermal grease was sandwiched between the silicon substrate and the sample holder to enhance thermal contact. Nitrogen adsorption isotherms were performed on a Quantachrome Autosorb 1 surface area analyzer, and samples were outgassed at 120 °C for at least 15 h prior to measurement. Thermal analyses were performed on a TA Instruments SDT 2960 Integrated TGA/DSC analyzer with a heating rate of 10 °C min^{-1} under a flow of nitrogen or oxygen. Calcinations were performed using a Lindberg 1200 °C three-zone furnace with a heating rate of 10 °C min^{-1} under a flow of oxygen and the temperature was held constant for 4 h. GC analyses were performed with an HP 6890 GC system using a methyl siloxane capillary (50.0 m × 320 μm × 1.05 μm nominal) and integration was performed relative to dodecane.

3. Results and discussion

3.1. Synthesis and characterization of $[(^tBuO)_2Ti\{\mu\text{-}O_2Si[OSi(O^tBu)_3]_2\}]_2$ (1)

The dimeric titanium complex **1** was prepared by reaction of a pentane solution of

$$\mathrm{Ti(O^tBu)_4} + [(^t\mathrm{BuO})_3\mathrm{SiO}]_2\mathrm{Si(OH)_2} \xrightarrow{\text{pentane}} \underset{\mathbf{1}}{(1/2)\,[(^t\mathrm{BuO})_2\mathrm{Ti}\{\mu\text{-}\mathrm{O_2Si}[\mathrm{OSi}(\mathrm{O^tBu})_3]_2\}]_2} + 2\,^t\mathrm{BuOH} \quad (3)$$

$[(^t\mathrm{BuO})_3\mathrm{SiO}]_2\mathrm{Si(OH)_2}$ [24] (1 equiv) with $\mathrm{Ti(O^tBu)_4}$ (Eq. (3)). Analytically pure, colorless crystals of air- and moisture-sensitive **1** were obtained by crystallization from pentane/toluene at −78 °C. The solution ^{1}H NMR spectrum of **1** in benzene-d_6 contains two resonances at 1.59 and 1.55 ppm corresponding to the $\mathrm{Si(O^tBu)_3}$ and $\mathrm{Ti(O^tBu)_3}$ groups, respectively. Likewise, the solution ^{13}C NMR spectrum of **1** in benzene-d_6 revealed one set of resonances for the *tert*-butoxy groups of the siloxy ligand and one set of resonances for the *tert*-butoxy groups bound to titanium. Attempts to obtain a solution ^{29}Si NMR spectrum of **1** in various solvents were unsuccessful due to the limited solubility of the highly crystalline precursor, but a solid-state MAS ^{29}Si NMR spectrum was successfully obtained in lieu of a solution spectrum. As expected the spectrum contains two resonances, at −100 ppm ($\mathrm{Si(O^tBu)_3}$) and −116 ppm ($\mathrm{Si(OTi)_2}$).

The structure of **1** was unequivocally determined by single-crystal X-ray structure analysis ([26, Supporting information]). Crystals of **1** generally diffracted poorly, and therefore the structure was only determined to a resolution of 0.95 Å. Although accurate metric parameters could not be obtained from the structural refinement, the data are of sufficient quality to determine the connectivity of **1**. It is clear that the two titanium centers exhibit pseudo-tetrahedral geometries, as shown in the ORTEP diagram of **1** (Fig. 1). Abe and Kijima have previously reported the synthesis of the related $[(^i\mathrm{PrO})_2\mathrm{Ti}\{\mu\text{-}\mathrm{O_2Si}[\mathrm{OSi}(\mathrm{O^tBu})_3]_2\}]_2$ complex, however no single-crystal X-ray structure was reported [27].

Complex **1** is useful as a spectroscopic model for pseudo-tetrahedral Ti(IV) centers in titania–silica materials. The FT-IR spectrum of **1** exhibits strong Si–O–Si and Si–O–C overlapping bands centered at 1068 cm^{-1}. In addition, a strong band centered at 974 cm^{-1} is observed for the Ti–O–Si linkage [5,11,28]. The band observed for the asymmetric Ti-O–Si stretch is similar in energy to that observed for $\mathrm{Ti[OSi(O^tBu)_3]_4}$ (925 cm^{-1}). Additionally, by solution UV–vis spectroscopy (in dry pentane solution), a strong

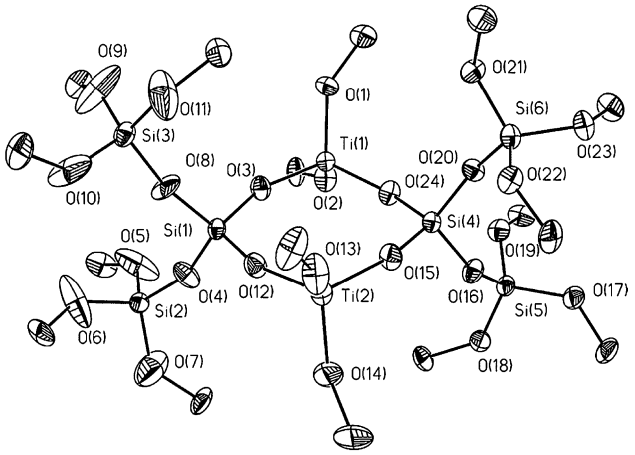

Fig. 1. ORTEP diagram of $[(^tBuO)_2Ti\{\mu\text{-}O_2Si[OSi(O^tBu)_3]_2\}]_2$ (**1**) at the 50% probability level. Terminal methyl groups and hydrogen atoms have been omitted for clarity.

absorption at λ_{max} = 216 nm is observed for a ligand to Ti(IV) charge transfer band (LMCT) for **1** [9,29]. The absorption observed for the LMCT band is slightly blue-shifted relative to that observed for $Ti[OSi(O^tBu)_3]_4$ (λ_{max} = 227 nm), presumably as a result of the different coordination environments of the two titanium centers (i.e., $Ti(OSi)_2(OR)_2$ versus $Ti(OSi)_4$). The molecular precursor **1** was also analyzed by X-ray photoelectron spectroscopy (XPS) to probe the chemical environment of titanium. The binding energy of the Ti $2p_{3/2}$ peak is centered at approximately 461 eV, which is ca. 2 eV higher than the binding energy reported for titanium in an octahedral oxygen environment [30].

3.2. Thermolytic conversion of *1* to $TiO_2{\cdot}3SiO_2$

The thermogravimetric analysis (TGA) of **1** under a flow of nitrogen revealed a precipitous weight loss corresponding to stoichiometric formation of $TiO_2{\cdot}3SiO_2$ (Fig. 2). The onset temperature of decomposition is ca. 140 °C, which is over 100 °C lower than that for the related $Ti[OSi(O^tBu)_3]_4$ complex [21]. The ceramic yield (33.3%) after heating **1** to

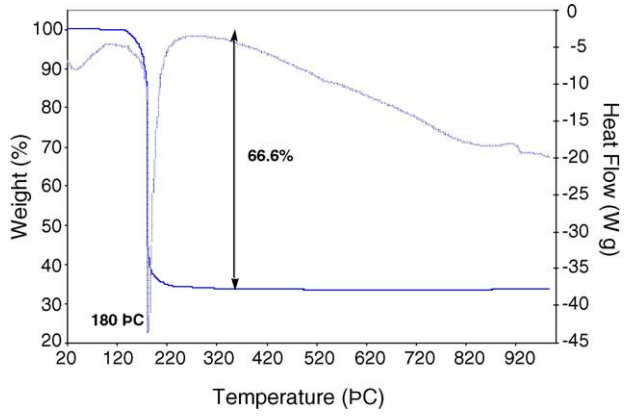

Fig. 2. TGA/DSC traces for **1** under a flow of nitrogen, with a heating rate of 10 °C min^{-1}.

1000 °C corresponds to quantitative formation of $TiO_2{\cdot}3SiO_2$ material (theoretical yield, 33.3%). Analysis of the thermal decomposition by differential scanning calorimetry (DSC) revealed the occurrence of a strong endothermic transition centered at 180 °C, corresponding to the precipitous weight loss from decomposition. The solubility of **1** in organic solvents also makes it possible to carry out the thermal decomposition in solution. The decomposition of **1** was monitored by solution ^1H NMR spectroscopy by quantifying the soluble decomposition products against an internal standard (ferrocene) in benzene-d_6. After 24 h at 160 °C, **1** had been completely converted and the observed products were isobutylene (11 equiv) and *tert*-butanol (1 equiv).

Bulk samples of $TiO_2{\cdot}3SiO_2$ were obtained by heating a toluene solution of **1** (0.06 M) in a sealed Parr reactor under an atmosphere of nitrogen for 24 h. This preparation yielded transparent monolithic gels that possess a slight yellow tint. The gels were air-dried for 1 week, washed with pentane and toluene, and then air-dried again overnight. The final xerogels (off-white in color) were then ground into a fine powder and dried in vacuo (120 °C) for 12 h to yield the as-prepared $TiO_2{\cdot}3SiO_2$ material. Calcination of the xerogel to 500 °C under a flow of oxygen (heated at 10 °C min^{-1}) yielded a material designated as $TiO_2{\cdot}3SiO_2$-500.

3.3. Characterization of $TiO_2{\cdot}3SiO_2$ materials

The carbon content for $TiO_2{\cdot}3SiO_2$ was found to be 6.7% by combustion analysis. After calcination, most of the carbon in $TiO_2{\cdot}3SiO_2$-500 was removed (<1%) to yield a pure-white xerogel. Thermogravimetric analysis of $TiO_2{\cdot}3SiO_2$ in oxygen with a heating rate of 10 °C min^{-1} revealed a mass loss of 9.5% up to 350 °C that probably corresponds to physisorbed and chemisorbed water in addition to residual organic species [31]. The silicon environments of $TiO_2{\cdot}3SiO_2$ were examined by solid-state ^{29}Si CP MAS NMR spectroscopy. The ^{29}Si CP MAS NMR spectrum of $TiO_2{\cdot}3SiO_2$ reveals a resonance centered at −101 ppm (with a distinct shoulder at −109 ppm) that spans the chemical shift range for Q^2, Q^3, and Q^4 silicon environments.

The crystallization behavior of $TiO_2{\cdot}3SiO_2$ was monitored by powder X-ray diffraction (PXRD). As initially isolated, $TiO_2{\cdot}3SiO_2$ was amorphous by PXRD and electron diffraction and remained so after heating to 500 °C (10 °C min^{-1} under a flow of oxygen). After heating the xerogel to >800 °C (4 h, 10 °C min^{-1} under a flow of oxygen), small domains of anatase were observed as very broad peaks in the PXRD pattern. These diffraction peaks became more pronounced as the domain size increased after heating to 1000 °C under the same conditions. Analysis of $TiO_2{\cdot}3SiO_2$ by DSC revealed an exothermic transition with an onset at 815 °C (under oxygen) that corresponds to the crystallization of anatase, as confirmed by PXRD analysis. It has been reported that delayed crystallization of TiO_2 in titania–silica samples is correlated with homogeneity in the uncalcined sample [32]. Bulk TiO_2

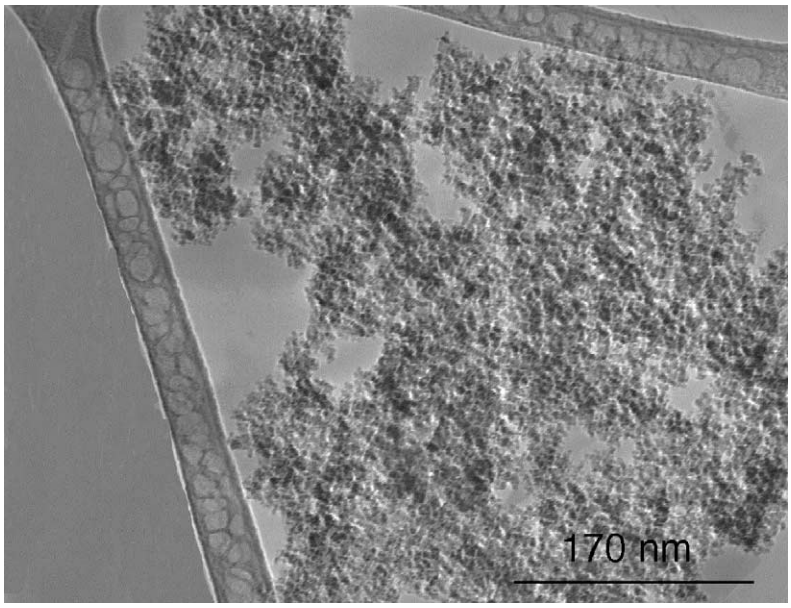

Fig. 3. TEM micrograph of $TiO_2{\cdot}3SiO_2$.

crystallizes into anatase at ca. 415 °C, whereas these materials delay crystallization until >800 °C [33].

Transmission electron microscopy (TEM) studies of $TiO_2{\cdot}3SiO_2$ revealed aggregates of fine granules with a wide range of particle sizes (Fig. 3). To probe the chemical composition and homogeneity of the materials, energy-dispersive X-ray spectroscopy (EDS) was used to assess the stoichiometry of silicon and titanium in the xerogel. EDS profiles taken from large (18–30 nm) areas revealed the Si/Ti ratio to be 4.1 ± 0.7:1, which is close to the expected value of 3:1 but high in silicon. In addition, local EDS spectroscopy at high spatial resolution was used to assess the distribution of silicon and titanium. EDS profiles taken from 20 random local areas (14 Å beam spot size) gave a Si/Ti ratio of 3.6 ± 0.4:1. This confirms that the ratio of silicon to titanium is relatively constant for these xerogels, even on the scale of 14 Å, over the bulk of the xerogel. It appears that the distribution of silicon and titanium throughout the xerogel is fairly constant, however the slight excess of silicon suggests that there might be small domains of TiO_2 that were not detected by PXRD or XPS (vide infra). EDS profiles taken from 18.0 nm regions of $TiO_2{\cdot}3SiO_2$-500 revealed the Si/Ti ratio to be 4.5:1, which is on average slightly more silicon rich than the uncalcined material. Surface elemental composition analysis (by XPS) of 10 randomly selected particles of $TiO_2{\cdot}3SiO_2$ gave an average Si/Ti ratio of 11.0 ± 0.6:1, which was fairly consistent for each measurement. It has been previously reported that titanium-rich titania–silica materials are often titanium-poor on the surface [30].

The FT-IR spectrum of $TiO_2{\cdot}3SiO_2$ shows a characteristic band at 944 cm^{-1} that is assigned as the asymmetric stretching mode of the Ti–O–Si linkage. Spectra of $TiO_2{\cdot}3SiO_2$-500 exhibit a band at 950 cm^{-1} that is assigned to the same stretching mode. FT-IR spectra taken of pure silica did not exhibit a distinct band in the region of 920–980 cm^{-1}. The observed bands at 940–950 cm^{-1} (Fig. 4) are generally thought to result from the overlap of two contributions (i.e., the Ti–O–Si asymmetric stretching mode at ca. 930 cm^{-1} and the Si–OH stretching mode at ca. 980 cm^{-1}). Thus, its observation is not a definitive indication of the presence of isolated Ti(IV) sites [34].

Diffuse reflectance UV–vis spectroscopy (DRUV–vis) is a useful corroborative tool used in conjunction with FT-IR spectroscopy to suggest the presence of four-coordinate Ti(IV) sites. The DRUV–vis spectrum of $TiO_2{\cdot}3SiO_2$ (taken under ambient air conditions) exhibits a strong absorption at $\lambda_{max} = 264$ nm for the oxygen to Ti(IV) charge transfer band (LMCT). Similarly, the DRUV–vis spectrum of $TiO_2{\cdot}3SiO_2$-500 contains an absorption at $\lambda_{max} = 279$ nm. Absorption maxima in the range of 210–240 nm are attributed to a LMCT for true four-coordinate Ti(IV), as evidenced by the molecular precursor **1** ($\lambda_{max} = 216$ nm). Absorption bands in the

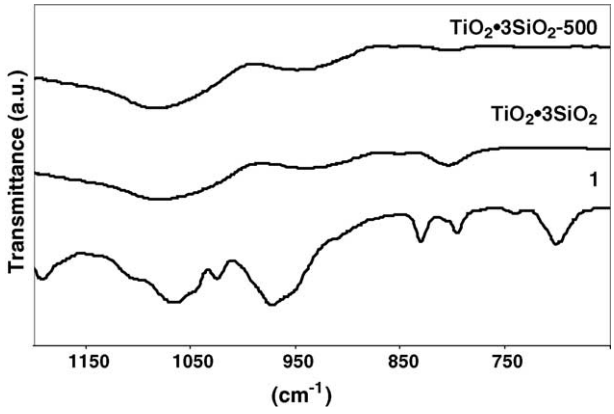

Fig. 4. FT-IR spectra of **1**, $TiO_2{\cdot}3SiO_2$, and $TiO_2{\cdot}3SiO_2$-500.

region of 250–280 nm have been assigned to centers with water coordinated to isolated Ti(IV) sites, or to oligomerized TiO_2 [35]. Bulk anatase displays an absorption maximum at ca. 330 nm [29]. Thus, DRUV–vis spectroscopy indicates that these materials (under ambient air atmosphere) possess titanium centers that may be described as four-coordinate $Ti(OSi)_4$ species, possibly with some degree of water coordination ($Ti(OSi)_4(H_2O)_n$) and/or octahedral TiO_2 oligomerization. XPS studies of $TiO_2{\cdot}3SiO_2$ revealed the appropriate Ti $2p_{3/2}$ peak at a binding energy of 461 eV, which corresponds to tetrahedral Ti(IV) and is in agreement with the binding energy of the Ti $2p_{3/2}$ peak observed for **1**. Similarly, the same binding energy of the Ti $2p_{3/2}$ peak was observed for $TiO_2{\cdot}3SiO_2$-500. The observed binding energies at 461 eV do not preclude the possibility of a small contribution from octahedral Ti(IV) at 458 eV; however, no obvious shoulder is present in the spectra.

Nitrogen porosimetry was used to evaluate the pore structures and surface areas of the new materials. The adsorption–desorption data correspond to type IV isotherms (Fig. 5) [36], suggesting some mesoporosity; however, much of the porosity appears to result from micopores with radii <20 Å. The isotherm for $TiO_2{\cdot}3SiO_2$ possesses an H3 hysteresis (IUPAC) that is indicative of an aggregate material (i.e., loosely coherent particles), and the steep rise in adsorbed volume at relative pressure $(P/P_o) > 0.8$ indicates textural porosity [36,37]. The materials were found to have relatively high BET surface areas ranging from 290 $m^2\,g^{-1}$ (pore volume of 1.3 $cm^3\,g^{-1}$) for $TiO_2{\cdot}3SiO_2$ to 320 $m^2\,g^{-1}$ (pore volume of 1.0 $cm^3\,g^{-1}$) for $TiO_2{\cdot}3SiO_2$-500. The concentration of Brønsted acid sites (OH) was determined by quantification of the amount of toluene evolved after reaction of the xerogels with $Mg(CH_2Ph)_2{\cdot}2THF$ [38]. $TiO_2{\cdot}3SiO_2$ was observed to possess an OH coverage of $1.7 \pm 0.1\ nm^{-2}$, while $TiO_2{\cdot}3SiO_2$-500 had an OH coverage of $4.0 \pm 0.4\ nm^{-2}$. The higher number of OH sites for the latter sample may result from a restructuring of the surface upon calcination, perhaps by decomposition of residual Si–O^{t}Bu groups (6.7% carbon content) to Si–OH. The presence of Si–O^{t}Bu groups in uncalcined $ZrO_2{\cdot}4SiO_2$ xerogels has been previously observed by ^{13}C CP MAS NMR spectroscopy [38].

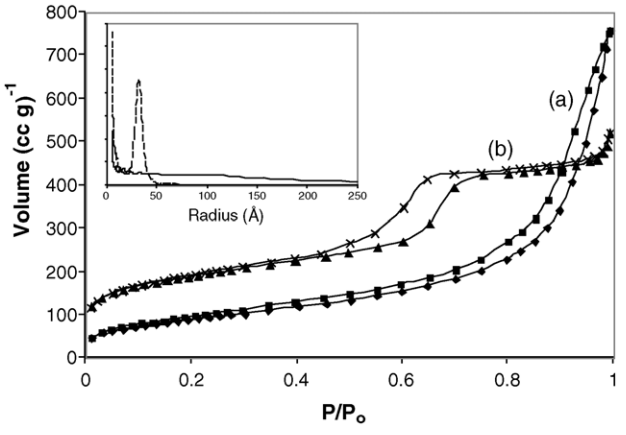

Fig. 5. Nitrogen adsorption–desorption isotherm for $TiO_2{\cdot}3SiO_2$ (a) and Ti_2SBA15(1.58) (b). Pore size distributions calculated from the adsorption isotherm branch are shown as an inset (— for $TiO_2{\cdot}3SiO_2$ and - - - for Ti_2SBA15(1.58)).

3.4. Grafting of **1** onto the SBA-15 surface

The mesoporous silica SBA-15 was prepared according to the literature procedure [25]. Precursor **1** was grafted onto the silica surface by adding a pentane solution of **1** to a stirred pentane suspension of SBA-15 under nitrogen at room temperature. The desired wt% Ti loading was controlled by varying the concentration of **1** in the added pentane solution. After 15 h, the pentane was filtered off and the resulting material was washed with pentane and dried in vacuo at room temperature to yield Ti_2SBA15(x) (where x is the wt% of Ti). Additional catalysts were prepared by calcination of the grafted materials to 300 °C (10 °C min^{-1}, under flowing oxygen) to yield Ti_2SBA15(x)-300 samples. Titanium analyses by inductively coupled plasma atomic emission spectroscopy determined that the two samples studied here possessed Ti wt% values of 0.17% and 1.58%. As expected, the grafted materials have surface areas (600 $m^2\,g^{-1}$) that are slightly reduced relative to that of the SBA-15 support; however, the mesostructured architecture was retained as evidenced by retention of the low-angle (1 0 0) reflection in the powder X-ray diffraction pattern. The adsorption–desorption data corresponds to a type IV isotherm, characteristic of mesoporous SBA-15 materials (Fig. 5) [25]. The pore size distribution was observed to be relatively narrow and the average pore radius, as determined by the nitrogen adsorption isotherm, was 33 Å. The pore structure of Ti_2SBA15 stands in contrast with that of the $TiO_2{\cdot}3SiO_2$ xerogels in that it has a well-defined, mesoporous, hexagonally ordered pore structure.

Solution ^{1}H NMR spectroscopy was used to monitor the grafting chemistry of **1** onto the silica surface. The reaction of surface Si–OH groups with a solution of a large excess of **1** should result in the elimination of *tert*-butanol (reaction of the Ti–OC linkage) or $[(^t\text{BuO})_3\text{SiO}]_2\text{Si(OH)}_2$ (reaction of the Ti–OSi linkages). The elimination products of grafting **1** onto SBA-15 in benzene-d_6 were indeed identified by ^{1}H NMR spectroscopy to be *tert*-butanol and $[(^t\text{BuO})_3\text{SiO}]_2\text{Si(OH)}_2$; however, only 0.1–0.2 equiv of each was observed (per equiv of grafted precursor **1**). The measured amounts of elimination products indicate a Ti loading of ca. 3.4 wt% (assuming loss of one elimination product per grafted molecule of **1**), whereas a loading of 9.0 wt% was suggested by the amount of **1** that was grafted to the silica surface (versus a ferrocene standard). Thus, it appears that some amount of precursor **1** may graft onto the surface of SBA-15 without the concomitant formation of elimination products. Indeed, this seems quite likely if reaction with a surface Si–OH group results in opening of the chelate ring formed by the bridging $[(^t\text{BuO})_3\text{SiO}]_2\text{SiO}_2{}^{2-}$ ligand. Another explanation for these results is that the elimination products become bound to the silica surface or Ti(IV) centers, and are thus not observed

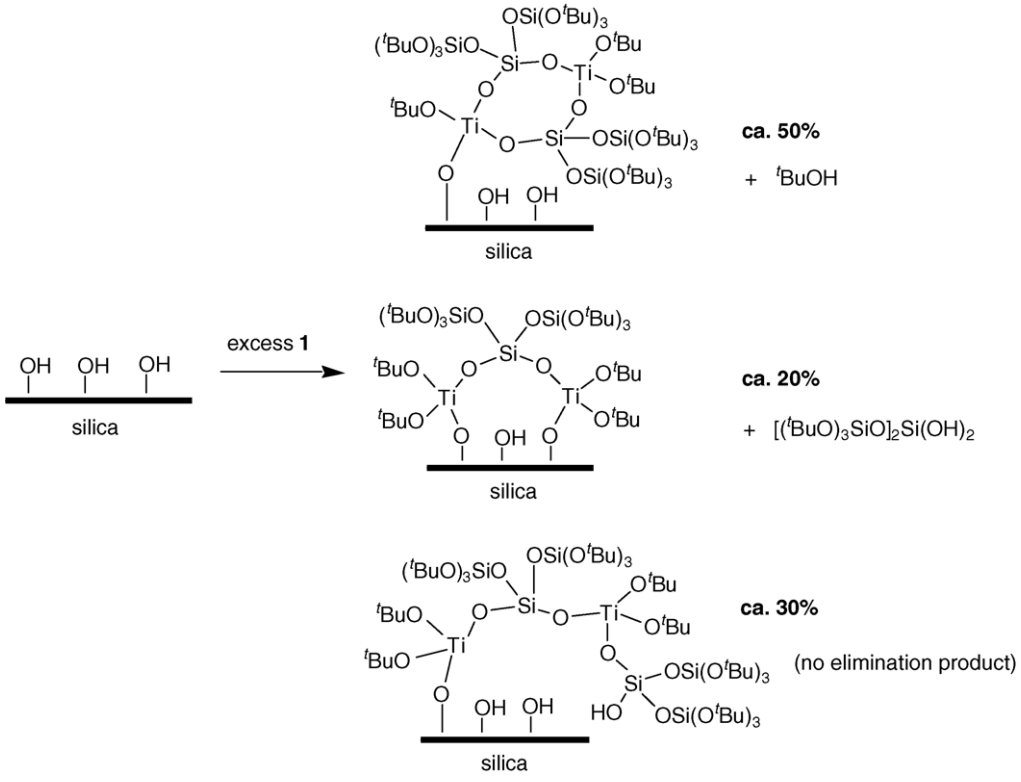

Scheme 1.

by NMR spectroscopy. The concentrations of *tert*-butanol and $[(^tBuO)_3SiO]_2Si(OH)_2$ are completely unaffected by the presence of SBA-15, as determined by ^1H NMR spectroscopy (in benzene-d_6). In addition, washing the grafted material with liberal amounts of pentane did not result in the liberation of **1**, or further elimination products. Even under catalytic conditions (peroxide, toluene, 65 °C), there was no evidence for the leaching of **1** into solution (vide infra). In order to test whether *tert*-butanol coordinated to the Ti(IV) centers following elimination, an excess of dry pyridine was added after the grafting reaction had gone to completion, as excess pyridine should displace surface coordinated *tert*-butanol. The measured concentration of *tert*-butanol increases ca. 2.5-fold after pyridine addition, thus ca. 0.5 equiv (not 0.2 equiv) of *tert*-butanol are eliminated per grafted molecule of **1** with some remaining coordinated to the Ti(IV) sites. Based on these findings, it seems likely that the grafting of **1** produces site-isolated di-titanium centers on the silica surface. However, the exact structure of the surface-bound Ti(IV) species remains unknown due to the lack of spectroscopic handles. Proposed structures that correspond to adding a large excess of **1** to SBA-15 (as described above) are shown in Scheme 1.

3.5. Characterization of Ti(IV) sites in Ti_2SBA15 catalysts

DRUV–vis spectroscopy was used to elucidate the Ti(IV) environments in the Ti_2SBA15 catalysts (Fig. 6). The DRUV–vis spectra of Ti_2SBA15(0.17) and Ti_2SBA15(1.58) taken under ambient conditions in air reveal LMCT bands with λ_{max} values of 250 and 252 nm, respectively. As discussed previously, this indicates the presence of isolated, four-coordinate Ti(IV) sites with perhaps some degree of water coordination $(Ti(OSi)_n(OR)_{4-n}(H_2O)_m)$. It is unlikely that there is oligomerized TiO_2 present in the Ti_2SBA15 catalysts because of their low titanium weight loading and low calcination temperatures (25–300 °C). The λ_{max} values of the LMCT bands for these catalysts are blue shifted relative to

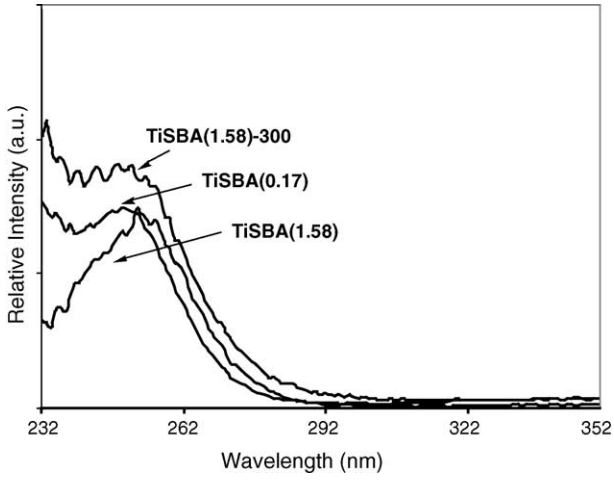

Fig. 6. DRUV–vis spectra of Ti_2SBA15(0.17), Ti_2SBA15(1.58), and Ti_2SBA15(1.58)-300 taken in ambient conditions.

those of $TiO_2{\cdot}3SiO_2$ and $TiO_2{\cdot}3SiO_2$-500, as expected for materials with authentic surface-supported Ti(IV) centers. Calcination of these catalysts did not significantly change the Ti(IV) environment, as determined by DRUV–vis spectroscopy. Thus, the λ_{max} value for Ti_2SBA15(1.58)-300 was found to be 248 nm.

Photoluminescence (PL) spectroscopy was used to further explore the nature of the supported Ti(IV) centers in the Ti_2SBA15 catalysts. It has been previously reported that a complex luminescence profile (400–600 nm) is observed for Ti(IV)/SiO_2 materials with excitation energies in the range of 250–350 nm [39,40], as observed for TS1 [41,42], Ti–Y [43], Ti-β [44], and TiMCM-41 [45]. The observed emission is reported to result from radiative decay of the charge transfer state to the ground state (O^{-}–$Ti^{3+} \rightarrow O^{2-}$–$Ti^{4+}$) for Ti(IV). A series of emission spectra (collected at 4.5–5.5 K, $\sim 1 \times 10^{-5}$ Torr) were obtained with an excitation wavelength of 325 nm (Fig. 7). For Ti_2SBA15 (both 0.17 and 1.58 wt% Ti), a broad, non-Gaussian emission in the range of 400–700 nm was observed. The spectrum for Ti_2SBA15 contains two distinct emission features at ca. 422 and 505 nm, implying the presence of two different emission centers in the material. Both the high and low energy emissions display intense and resolved vibrational modes (at 407 and 426 nm for the high energy emission center and at 491 and 523 nm for the low energy emission center). Stiegman and co-workers have also observed the presence of two emission features at similar energies for TS1, with the lower energy emission at ca. 500 nm being assigned to Ti(IV) [41,42]. For comparison, PL spectra taken at room temperature (λ_{ex} = 325 nm, $\sim 1 \times 10^{-5}$ Torr) do not contain the fine structure observed at low temperature, as illustrated in Fig. 8.

The emission spectra of **1** and $Ti[OSi(O^tBu)_3]_4$ contain a feature at λ_{max} = 416 nm that is resolved into two modes at 408 and 424 nm. To investigate the emission origin of **1**, the silanol ligand $[(^tBuO)_3SiO]_2Si(OH)_2$ was excited at 325 nm,

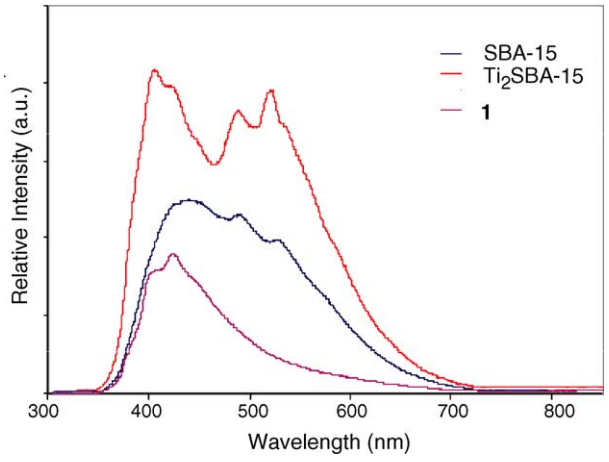

Fig. 7. Low temperature photoluminescence spectra of Ti_2SBA15(1.58), SBA-15, and molecular precursor **1**. The emission spectra were obtained by exciting the samples with λ_{ex} = 325 nm (50 scans, 4.5–5.5 K, and 1×10^{-5} Torr).

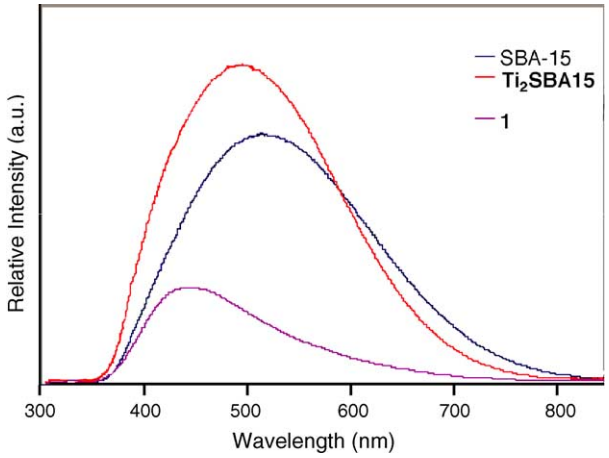

Fig. 8. Room temperature photoluminescence spectra of Ti_2SBA15(1.58), SBA-15, and molecular precursor **1**. The emission spectra were obtained by exciting the samples with λ_{ex} = 325 nm (50 scans, 298 K, and 1×10^{-5} Torr).

and, surprisingly, a very similar emission lineshape to that for **1** is observed. Thus, it appears that little, if any, of the emission observed for the molecular model complex **1** results from Ti(IV). The emission spectrum of ungrafted SBA-15 contains two features centered at 443 nm and ca. 508 nm, with the low energy emission resolved into two modes at 492 and 531 nm. Stiegman and co-workers reported several forms of silica exhibiting emissions with λ_{max} of ca. 420 nm, which they postulate as originating from trace metal impurities in the silica (i.e., Sn and Ge) [41,42]. Additionally, Stiegman and co-workers attribute the low energy emission (at ca. 500 nm) to Ti(IV) sites. In our system, it seems likely that the emissions at 420–440 nm observed for **1**, SBA-15, and Ti_2SBA15 are from non-titanium metal impurities, as previously assigned by Stiegman and co-workers[41,42]. The low energy emission we observe at λ_{max} of 505–508 nm is most likely emission from Ti(IV), as previously assigned [41,42]. The low intensity vibrational modes observed at λ_{max} = 508 nm for SBA-15 are possibly a result of Ti(IV) contamination (<20 ppm by ICP-AES) from the SBA-15 preparation. PL spectra of an ultrapure SBA-15 (0.48 ppm Ti) displayed a different lineshape to that of the less pure SBA-15, with no resolved vibrational modes in the low energy region. In summary, PL spectroscopy seems to confirm the presence of supported Ti(IV) on Ti_2SBA15, as indicated by intense vibrational modes at 491 and 523 nm. These modes are also observed in as-prepared SBA-15 as less intense bands at 492 and 531 nm, and presumably the small amount of titanium in this sample originates from impurities in the reagent grade $Si(OEt)_4$ and HCl starting materials used to prepare it.

3.6. Catalytic epoxidation of cyclohexene

Samples of $TiO_2{\cdot}3SiO_2$, $TiO_2{\cdot}3SiO_2$-500, Ti_2SBA15-(0.17), Ti_2SBA15(1.58), and Ti_2SBA15(1.58)-300 were all found to exhibit catalytic activity for the epoxidation of cyclohexene to cyclohexene oxide with cumene hydroperoxide

(CHP) or *tert*-butyl hydroperoxide (TBHP) as the oxidant, in toluene at 65 °C. To compare the activities for these heterogeneous catalysts, results were standardized with respect to the mass of catalyst used (0.035 g). In control experiments with $TiO_2{\cdot}3SiO_2$ and no TBHP (or CHP), or with TBHP (or CHP) and no catalyst, no cyclohexene oxide product was observed by gas chromatography (GC) analysis. To determine whether the catalytic species leached into solution during a typical run, a sample of $TiO_2{\cdot}3SiO_2$ and cyclohexene in toluene was heated to 65 °C for 1 h and then filtered via cannula while still hot, 10 min after the addition of oxidant. Samples analyzed by chromatography after filtration and 2 h at 65 °C indicated that no further cyclohexene oxide was produced, suggesting that leaching of a catalytically active titanium species into solution was negligible. No leaching of catalytically active species from the Ti_2SBA15 catalysts was observed after similar hot-filtration experiments. Furthermore, no appreciable catalytic activity was observed with as-prepared SBA-15. Catalysts that can be regenerated by calcination (e.g., $TiO_2{\cdot}3SiO_2$-500 and Ti_2SBA15(1.58)-300) retain at least 80% of their original activity in the epoxidation of cyclohexene (>98% selective for cyclohexene oxide) upon recycling and re-calcination.

The $TiO_2{\cdot}3SiO_2$ catalyst is active for epoxidation with both TBHP and CHP as the oxidant at 65 °C in toluene, yielding 8.6% (TBHP) and 14.1% (CHP) of cyclohexene oxide after 2 h (relative to initial concentration of peroxide). Likewise, Ti_2SBA15(1.58) is an active epoxidation catalyst with both TBHP and CHP at 65 °C in toluene, yielding 31% (TBHP) and 71% (CHP) of cyclohexene oxide after 2 h (relative to initial peroxide concentration). Thus, the structure of the organic hydroperoxide has an extremely important role in determining the activity of the catalyst [46]. The epoxidation is significantly more efficient with CHP as the oxygen-transfer reagent. This is consistent with previous results from investigations of epoxidation catalysts derived from grafting $Ti[OSi(O^tBu)_3]_4$ or $(^iPrO)Ti[OSi(O^tBu)_3]_3$ onto SBA-15 [21,22].

The cyclohexene oxide formation is generally more rapid (regardless of oxidant or catalyst) over the first 30 min of reaction, and distinctly slower the remaining 90 min. After oxidation no crystallites of anatase were detected by PXRD, and the DRUV–vis λ_{max} values red-shift only ca. 10 nm even under aqueous conditions. More likely, the catalyst inactivation is attributed to increasing quantities of the alcohol by-product, which hinders formation of the catalytically active titanium–hydroperoxide species through competitive binding of the alcohol [1]. The selectivity of the oxidation for cyclohexene oxide was found to be in excess of 98% after 2 h, for both CHP and TBHP, in all cases.

A graph comparing the activities of the catalysts (on a per gram basis with CHP as oxidant) under identical conditions is shown in Fig. 9. The Ti_2SBA15 catalysts exhibited a higher activity for the production of cyclohexene oxide than the titania–silica xerogels. This is presumably a result of site-isolated Ti(IV) surface centers that are present

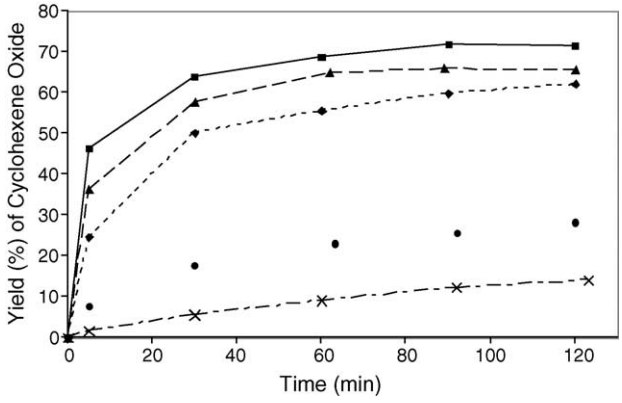

Fig. 9. Yield of cyclohexene oxide relative to initial CHP concentration as a function of time during the epoxidation of cyclohexene with 0.035 g of Ti_2SBA15(1.58) (■), Ti_2SBA15(0.17) (▲), Ti_2SBA15(1.58)-300 (♦), $TiO_2{\cdot}3SiO_2$-500 (●), $TiO_2{\cdot}3SiO_2$ (×).

in the mesoporous Ti_2SBA15(0.17), Ti_2SBA15(1.58), and Ti_2SBA15(1.58)-300 catalysts, whereas the titania–silica xerogels possess considerable amounts of substrate-unavailable titanium throughout the silicate walls and in the micropores of the material, in addition to a greater degree of titania oligomerization (as evidenced by DRUV–vis spectroscopy). It is interesting to note that the wt% loading of Ti did not have a dramatic effect on the catalytic activity for the Ti_2SBA15 catalysts, with the higher titanium content being only slightly more active. The calcined Ti_2SBA15(1.58)-300 catalyst exhibited a slightly lower catalytic activity than the uncalcined Ti_2SBA15(1.58), which is consistent with previous results [22]. Conversely, calcination of the amorphous titania-silica xerogel (i.e., $TiO_2{\cdot}3SiO_2$-500) resulted in a substantially higher catalytic activity as compared to the uncalcined $TiO_2{\cdot}3SiO_2$ xerogel. In this case, it is possible that calcination removes residual organic material thereby activating the titanium centers in the catalyst [21].

To make further comparisons between the different catalysts investigated here, turnover frequencies (TOFs), defined as moles of epoxide per mole of Ti(IV) per hour, were determined. The results are illustrated in Fig. 10a, which compares the catalyst efficiencies for both the titania–silica xerogels and the Ti_2SBA15 catalysts. Since a considerable amount of the titanium in $TiO_2{\cdot}3SiO_2$ and $TiO_2{\cdot}3SiO_2$-500 is presumably substrate unavailable, TOFs were also calculated on a mass basis (moles of epoxide per mass of catalyst per hour, Fig. 10b).

The initial rates of the epoxidation of cyclohexene for the different catalysts were calculated on a per gram basis over the first 5 min of the reactions (Table 1). The initial rates for $TiO_2{\cdot}3SiO_2$ and $TiO_2{\cdot}3SiO_2$-500 are significantly lower than those observed for the Ti_2SBA15 catalysts. Again, these results indicate that the catalysts with surface-bound Ti(IV) sites in the mesopores of Ti_2SBA15 are the most active. For comparison, the initial rate reported here for Ti_2SBA15(1.58) (14.23 mmol epoxide/g cat/min) is similar to that reported previously for single-site TiSBA15(1.64) (ini-

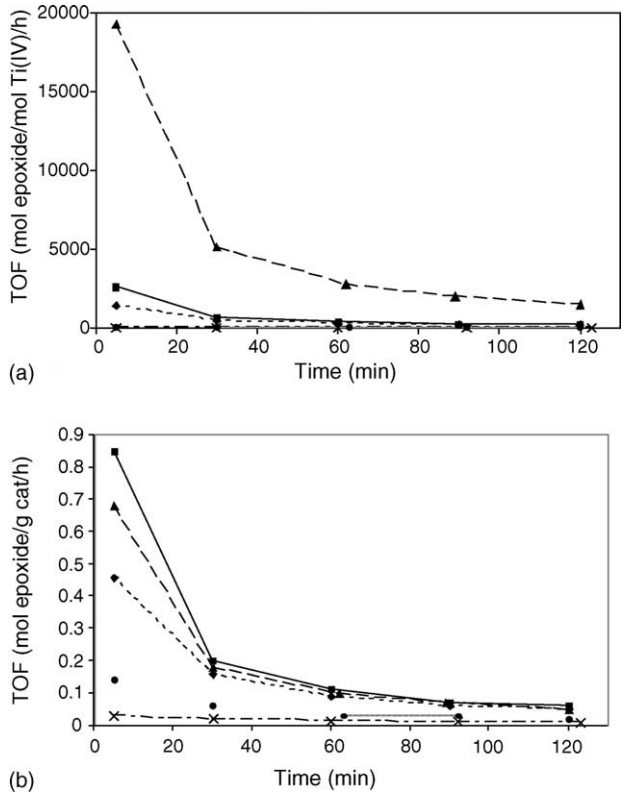

Fig. 10. Turnover frequencies (TOFs) as a function of time during the epoxidation of cyclohexene with Ti_2SBA15(1.58) (■), Ti_2SBA15(0.17) (▲), Ti_2SBA15(1.58)-300 (♦), $TiO_2{\cdot}3SiO_2$-500 (●), $TiO_2{\cdot}3SiO_2$ (×). (a) TOF = moles cyclohexene oxide per moles Ti(IV) per hour. (b) TOF = moles cyclohexene oxide per gram catalyst per hour.

tial rate = 11.30 mmol epoxide/g cat/min), prepared by grafting (^{i}PrO)Ti[OSi(O^{t}Bu)$_3$]$_3$ onto SBA-15 [22]. This provides evidence that the catalytic activity for Ti_2SBA15(1.58) materials derived from grafting a dimeric titanium complex onto SBA-15 is comparable to a material with a similar wt% Ti(IV) derived from grafting a monomeric titanium complex onto SBA-15. Moreover, the observed initial rate for cyclohexene epoxidation using Ti_2SBA15(1.58) and CHP is considerably higher than using TaSBA15(1.51) with CHP under identical conditions (initial rate = 4.25 mmol epoxide/g cat/min) [23]. Potential differences in observed rates caused by diffusion effects and particle size differences were not examined. However, the mesoporous catalysts all possess similar surface areas, pore sizes, and particle sizes.

Table 1
Comparison of initial rates[a] in epoxidation of cyclohexene calculated over the first 5 min of the reaction (65 °C)

Catalyst	Initial rate (mmol epoxide/g cat/min)
$TiO_2{\cdot}3SiO_2$	0.53[b]
$TiO_2{\cdot}4SiO_2$ [21]	1.38
$TiO_2{\cdot}3SiO_2$-500	2.40
Ti_2SBA15(0.17)	11.36
TiSBA15(1.64) [22]	11.30[c]
TaSBA15(1.51) [23]	4.25
Ti_2SBA15(1.58)	14.23
Ti_2SBA15(1.58)-300	7.71
5 wt% Ti(IV)/SiO_2 [11]	2.95
10 wt% Ti(IV)/SiO_2 [11]	6.01

[a] Initial rate measured as the slope of the tangent to the plot of concentration vs. time at $t = 0$, normalized per g of catalyst.
[b] Substrate/catalyst (wt) = 57.9; substrate/oxidant (mol) = 4.5; toluene solvent.
[c] Initial rate measured over 10 min.

It has been reported that TS1 as well as amorphous titanosilicates are active in the oxidation of benzene to phenol using aqueous hydrogen peroxide as the oxidant [47,48]. We therefore attempted the oxidation of benzene to phenol, mimicking conditions reported in the literature (temperature = 60 °C; substrate/catalyst (wt) = 10; substrate/H_2O_2 (mol) = 3; acetonitrile as solvent) with $TiO_2{\cdot}3SiO_2$ and Ti_2SBA15(1.58) as catalysts. Unfortunately, both systems proved to be ineffective as catalysts for benzene oxidation, and no conversion to phenol was observed after 24 h.

4. Concluding remarks

The preparation and structural determination of a new dimeric molecular precursor, [(^{t}BuO)$_2$Ti{μ-O$_2$Si-[OSi(O^{t}Bu)$_3$]$_2$}]$_2$ (**1**), has been described. The pseudo-tetrahedral Ti(IV) sites in **1** make this compound an interesting model for $O_2Ti(OSiO)_2TiO_2$ titanium sites in silica, and a number of spectroscopic methods have been employed to characterize this structure (i.e., NMR, FT-IR, UV–vis, XPS, PL).

Compound **1** is a versatile reagent for both the preparation of bulk $TiO_2{\cdot}3SiO_2$ xerogels and the grafting of isolated Ti(IV) centers onto the surface of silica. Examination of the xerogel materials by XPS, FT-IR spectroscopy, and DRUV–vis spectroscopy suggests that the Ti(IV) exists mainly as four-coordinate Ti(IV) with some degree of water coordination ($Ti(OSi)_4(H_2O)_n$) and/or TiO_2 oligomerization. Furthermore, a convenient method for introducing site-isolated Ti(IV) onto SBA-15 was described. Spectroscopic evidence (DRUV–vis, PL) suggests that these species remain site-isolated on the silica surface after grafting, and the stoichiometry strongly suggests the presence of dititanium centers. Upon calcination to 300 °C, the dimeric structure may degrade and diffuse into mono-titanium sites. The exact structure of the surface bound species (before or after calcination) is not known at this time.

The epoxidation catalysts derived from **1** exhibit activities comparable to those for previously reported high-performance titanium-containing catalysts. It was determined that the most active catalyst for the epoxidation of cyclohexene was Ti_2SBA15(1.58), using CHP as the oxidant in toluene at 65 °C. The initial rate measured over the first 5 min (14.23 mmol epoxide/g cat/min) for Ti_2SBA15(1.58) was found to be slightly better than that derived from a catalyst prepared by grafting the monomeric (^{i}PrO)Ti[OSi(O^{t}Bu)$_3$]$_3$ precursor onto SBA-15 (11.30 mmol epoxide/g cat/min). Additionally, for comparison, the initial rate is 4.8 and

2.4 times faster than those observed using 5 and 10 wt% Ti(IV)/SiO_2 catalysts, respectively, as reported by Hutter et al. for cyclohexene epoxidation [11]. Related group V catalysts also have shown catalytic activity for the non-selective oxidation of cyclohexene, with a 40–45% yield of oxidation products observed after 2 h using H_2O_2 with a NbMCM41 catalyst [49,50]. The use of organic peroxides with these catalysts was not commented upon, however. Similarly, TaSBA15 catalysts have demonstrated activity for the selective epoxidation of cyclohexene (ca. 6% yield of cyclohexene oxide after 2 h) using CHP as the oxidant [23].

The results presented here suggest that having site-isolated Ti(IV) (and not domains of TiO_2) is crucial in the design of a high-performance epoxidation catalyst; however, the use of a dinuclear Ti(IV) source does not hamper catalytic activity or selectivity. Previous results have suggested that the activity of amorphous titanosilicates is a function of titanium dispersion in the catalyst [51]. Work by Scott, Alper, and co-workers, however, demonstrated that the catalytically active surface-bound species from the reaction of $Ti(O^iPr)_4$ with silica is an oxo-bridged Ti–O–Ti dimer [52,53]. Taken in context with our results for the uncalcined Ti_2SBA15 catalysts, it seems that titanium dispersion on the surface may not be as critical as the presence of tetrahedral Ti(IV) sites (i.e., the titanium sites can be in close proximity to one another as long as domains of octahedral TiO_2 are not formed). This suggests that high activity and selectivity for olefin epoxidation could be achieved with a highly loaded catalyst surface that is stabilized against the nucleation of TiO_2.

5. Supporting information available

^{1}H, ^{13}C, and ^{29}Si NMR spectra, UV–vis spectrum, and XPS spectrum for **1**. Description of the structure determination for **1**. CCDC 267285 contains the supplementary crystallographic data for this paper. These data can be obtained free of charge from The Cambridge Crystallographic Data Center via http://www.ccdc.cam.ac.uk/data_request/cif.

Acknowledgments

This work was supported by the Director, Office of Energy Research, Office of Basic Energy Sciences, Chemical Sciences Division, of the U.S. Department of Energy under Contract No. DE-AC03-76SF00098. R.L.B. thanks the National Science Foundation for support with a NSF Graduate Fellowship. We thank P. Yu at the University of California, Davis and R. Nunlist at the University of California, Berkeley for the MAS NMR spectra and A. M. Stacy at the University of California, Berkeley for use of instrumentation (PXRD, DRUV–vis). We are grateful to A. Tolley and C. Song for technical assistance with electron microscopy and the National Center for Electron Microscopy for use of their microscopes. We are grateful to A. Stiegman for valuable discussions regarding the PL data.

Appendix A. Supplementary data

Supplementary data associated with this article can be found, in the online version, at doi:10.1016/j.molcata.2005.04.032.

References

[1] R.A. Sheldon, J. Mol. Catal. 7 (1980) 107.
[2] M.G. Clerici, G. Bellusi, U. Romano, J. Catal. 129 (1991) 159.
[3] M.G. Clerici, P. Ingallina, J. Catal. 140 (1993) 71.
[4] B. Notari, Adv. Catal. 41 (1996) 253.
[5] R. Hutter, D.C.M. Dutoit, T. Mallat, M. Schneider, A. Baiker, J. Chem. Soc., Chem. Commun. (1995) 163.
[6] M.A. Camblor, A. Corma, A. Martinez, J. Pérez-Pariente, J. Chem. Soc., Chem. Commun. (1992) 589.
[7] F. Chiker, F. Launay, J.P. Nogier, J.L. Bonardet, Green Chem. 5 (2003) 318.
[8] A. Tuel, L.G. Hubert-Pfalzgraf, J. Catal. 217 (2003) 343.
[9] T. Blasco, A. Corma, M.T. Navarro, J. Pérez-Pariente, J. Catal. 156 (1995) 65.
[10] K. Murata, Y. Liu, N. Mimura, M. Inaba, Catal. Commun. 4 (2003) 385.
[11] R. Hutter, T. Mallat, A. Baiker, J. Catal. 153 (1995) 177.
[12] P.E. Sinclair, C.R.A. Catlow, J. Phys. Chem. B 103 (1999) 1084.
[13] J.M. Thomas, G. Sankar, Acc. Chem. Res. 34 (2001) 571.
[14] W. Rupp, N. Hüsing, U. Schubert, J. Mater. Chem. 12 (2002) 2594.
[15] T. Gunji, T. Kasahara, Y. Abe, J. Sol-Gel Sci. Technol. 13 (1998) 975.
[16] R. Murugavel, P. Davis, V.S. Shete, Inorg. Chem. 42 (2003) 4696.
[17] L. Crouzet, D. Leclercq, P.H. Mutin, A. Vioux, Chem. Mater. 15 (2003) 1530.
[18] S.A. Holmes, F. Quignard, A. Choplin, R. Teissier, J. Kervennal, J. Catal. 176 (1998) 173.
[19] S.A. Holmes, F. Quignard, A. Choplin, R. Teissier, J. Kervennal, J. Catal. 176 (1998) 182.
[20] J. Notestein, E. Inglesia, A. Katz, J. Am. Chem. Soc. 126 (2004) 16478.
[21] M.P. Coles, C.G. Lugmair, K.W. Terry, T.D. Tilley, Chem. Mater. 12 (2000) 122.
[22] J. Jarupatrakorn, T.D. Tilley, J. Am. Chem. Soc. 124 (2002) 8380.
[23] R.L. Brutchey, C.G. Lugmair, L.O. Schebaum, T.D. Tilley, J. Catal. 229 (2005) 77.
[24] Y. Abe, I. Kijima, Bull. Chem. Soc. Jpn. 42 (1969) 1118.
[25] D. Zhao, Q. Huo, J. Feng, B.F. Chmelka, G.D. Stucky, J. Am. Chem. Soc. 120 (1998) 6024.
[26] Crystallographic data for **1**. Crystal dimensions: 0.15 mm × 0.13 mm × 0.07 mm. Crystal system: triclinic. Space group: $P\bar{1}$(#2). Unit cell dimensions and volume: $a = 13.559(2)$ Å, $b = 13.792(2)$ Å, $c = 28.391(4)$ Å, $\alpha = 100.686(2)^\circ$, $\beta = 93.024(2)^\circ$, $\gamma = 118.607(2)^\circ$, $V = 4518.4(10)$ Å^3. $\rho_{calc} = 1.148$ g cm^{-3}. Radiation: Mo Kα ($\lambda = 0.71069$ Å). Scan type: ω (0.3° per frame). Temperature of measurement: −151 °C. No. of reflections measured: total = 22828, unique = 14344. $R_{obs} = 0.077$, $R_{all} = 0.160$, w$R_2 = 0.188$, $GOF_{obs} = 1.173$.
[27] Y. Abe, I. Kijima, Bull. Chem. Soc. Jpn. 43 (1970) 466.
[28] M.A. Uguina, G. Ovejero, R. van Grieken, D.P. Serrano, M. Camacho, J. Chem. Soc., Chem. Commun. (1994) 27.
[29] S. Klein, B.M. Weckhuysen, J.A. Martens, W.F. Majer, P.A. Jacobs, J. Catal. 163 (1996) 489.

[30] T. Blasco, M.A. Camblor, J.L.G. Fierro, J. Pérez-Pariente, Microp. Mater. 3 (1994) 259.
[31] C.P. Jaroniec, M. Kruk, M. Jaroniec, A. Sayari, J. Phys. Chem. B 102 (1998) 5503.
[32] M. Andrianainarivelo, R. Corriu, D. Leclercq, P.H. Mutin, A. Vioux, J. Mater. Chem. 6 (1996) 1665.
[33] K. Okada, K. Katsumata, Y. Kameshima, A. Yasumori, J. Am. Ceram. Soc. 85 (2002) 2078.
[34] D.C.M. Dutoit, M. Schneider, A. Baiker, J. Catal. 153 (1995) 165.
[35] L. Marchese, T. Maschmeyer, E. Gianotti, S. Coluccia, J.M. Thomas, J. Phys. Chem. B 101 (1997) 8836.
[36] K.S.W. Sing, Pure Appl. Chem. 57 (1985) 603.
[37] P.T. Tanev, T.J. Pinnavaia, Chem. Mater. 8 (1996) 2068.
[38] R.L. Brutchey, J.E. Goldberger, T.S. Koffas, T.D. Tilley, Chem. Mater. 15 (2003) 1040.
[39] H. Yiamachita, Y. Ichihashi, M. Harada, G. Steward, M.A. Fox, M. Anpo, J. Catal. 158 (1996) 97.
[40] H. Yiamachita, Y. Ichihashi, M. Anpo, M. Hashimoto, C. Louis, M. Che, J. Phys. Chem. 100 (1996) 16041.
[41] A.S. Soult, D.D. Pooré, E.I. Mayo, A.E. Stiegman, J. Phys. Chem. B 105 (2001) 2687.
[42] A.S. Soult, D.F. Carter, H.D. Schreiber, L.J. van de Burgt, A.E. Stiegman, J. Phys. Chem. B 106 (2002) 9266.
[43] Y. Ichihashi, H. Yamashita, M. Anpo, Y. Souma, Y. Matsumura, Catal. Lett. 53 (1998) 107.
[44] K. Ikeue, H. Yamashita, M. Anpo, T. Takewaki, J. Phys. Chem. B 105 (2001) 8350.
[45] E. Gianotti, V. Dellarocca, L. Marchese, G. Martra, S. Coluccia, T. Maschmeyer, Phys. Chem. Chem. Phys. 4 (2002) 6109.
[46] R.A. Sheldon, J.A. van Doorn, C.W.A. Schram, A.J. de Jong, J. Catal. 31 (1973) 438.
[47] A. Keshavaraja, V. Ramaswamy, H.S. Soni, A.V. Ramaswamy, P. Ratnasamy, J. Catal. 157 (1995) 501.
[48] L. Balducci, D. Bianchi, R. Bortolo, R. D'Aloiso, M. Ricci, R. Tassinari, R. Ungarelli, Angew. Chem. Int. Ed. 42 (2003) 4937.
[49] M. Hartmann, A.M. Prakash, L. Kevan, Catal. Today 78 (2003) 467.
[50] B. Kilos, M. Aouine, I. Nowak, M. Ziolek, J.C. Volta, J. Catal. 224 (2004) 314.
[51] S. Klein, S. Thorimbert, W.F. Maier, J. Catal. 163 (1996) 476.
[52] A.O. Bouh, G.L. Rice, S.L. Scott, J. Am. Chem. Soc. 121 (1999) 7201.
[53] S. Sensarma, A.O. Bouh, S.L. Scott, H. Alper, J. Mol. Catal. 203 (2003) 145.